

Compact Modeling of the Switching Dynamics and Temperature Dependencies in TiO_x -Based Memristors—Part I: Behavioral Model

Dhirendra Vaidya¹, Shraddha Kothari, Thomas Abbey, Ali Khiat, Spyros Stathopoulos²,
Loukas Michalas³, Alexantrou Serb⁴, *Senior Member, IEEE*,
and Themis Prodromakis⁵, *Senior Member, IEEE*

Abstract—Memristor is a promising device as a fundamental building block for future unconventional system architectures such as neuromorphic computing, reconfigurable logic, and multibit memories. Therefore, to facilitate circuit design using memristors, accurate and efficient models spanning a wide range of programming voltages and temperatures are required. In the first part of this series, we propose a behavioral model for temperature dependence of nonvolatile switching dynamics of TiO_x memristors. We begin by describing pulsed resistance transients (PRTs) of the memristors and then we use a multistage methodology to establish bias and temperature dependence of the model parameters. The proposed model is then shown to accurately describe the PRT characteristics of $\text{Pt/TiO}_x/\text{Au}$ and $\text{Pt/TiO}_x/\text{Pt}$ memristors.

Index Terms—Behavioral model, metal oxide memristors, pulsed resistance transient (PRT) measurements, resistive RAMs switching dynamics, temperature dependence, TiO_x memristors.

I. INTRODUCTION

THE demonstration of memristors [1] in the past decade has opened up new research frontiers. These devices have been shown to be promising for applications in memory [2], neuromorphic computing [3]–[8], reconfigurable logic [9]–[11], sensing, and so on. To realize several potential applications, CMOS integration of memristor technology must be achieved. And for circuit designers to make use of this hybrid memristor-CMOS technology, it is important to capture the electrical characteristics of memristors with reasonable accuracy and computational efficiency.

In the past decade, several models have been proposed to describe the current–voltage (I – V) characteristics and mechanisms of change of the internal state variable(s) of mem-

ristors. These mechanisms are often related by modelers to electrochemical principles. For example, in the ion drift model, the internal state variable is interpreted as the position of the boundary between oxygen-rich and oxygen-deficient regions in the active layer oxide, whereas in TiO_x memristors, it is the barrier height or width at the electrode oxide interface [1], [12]–[17]. In general, internal state variable dictates the low field I – V relationships of memristor devices, whilst the rate of change of internal state variable is dictated by the applied programming or switching bias. Previously, it has been shown that, in general, for a variety of voltage-controlled memristor devices, a threshold exists for the programming voltage. The threshold voltage in this context is roughly defined as a voltage below which it is not possible to obtain a significant change in resistance in a practical time-frame. Therefore, it is possible to separate the two regimes, viz. a low-field regime or nonswitching regime and programming or switching regime for the modeling purposes. Such an approach was used in the VTEAM model [15]. More recently, it was shown that it is possible to describe resistive switching in memristors independent of the low-field device operation, that is, a physics-agnostic approach is used to define the state variable [14]. Because the model is behavioral and stresses speed over any other concerns, the memristor is modeled as having a single-state variable: its resistive state. Next, in the same work, a protocol involving pulsed resistance transient (PRT) measurement of the state variable (device resistance) at a fixed read-out voltage is proposed for extracting the parameters of the switching dynamics model.

In this work, we begin from the memristive model described in [14] and propose a method to extract improved switching dynamic components (leaving the static, i.e., nonswitching component the same) that also take into account the temperature dependence. The proposed components do not affect the static I – V relationship of the device. Moreover, model parameter extraction is carried out using the same form of PRT measurements proposed in [14], thus maintaining testing routine compatibility. The proposed model describes resistive switching in terms of fractional resistance change $d\Delta R/dt$ as opposed to simply dR/dt from our previous work. This allows us to reduce the size of the parameter space substantially.

Manuscript received July 12, 2021; accepted July 19, 2021. Date of publication August 26, 2021; date of current version September 22, 2021. This work was supported by FORTE, which is a UKRI Engineering and Physical Sciences Research Council Programme under Grant EP/R024642/1. The review of this article was arranged by Editor B. K. Kaushik. (Corresponding author: Dhirendra Vaidya.)

The authors are with the Centre for Electronics Frontiers, University of Southampton, Southampton SO17 1BJ, U.K. (e-mail: dhirendra22121987@gmail.com; t.prodromakis@soton.ac.uk).

Data is available on-line at <http://dx.doi.org/10.5258/SOTON/D1923>.

Color versions of one or more figures in this article are available at <https://doi.org/10.1109/TED.2021.3101996>.

Digital Object Identifier 10.1109/TED.2021.3101996

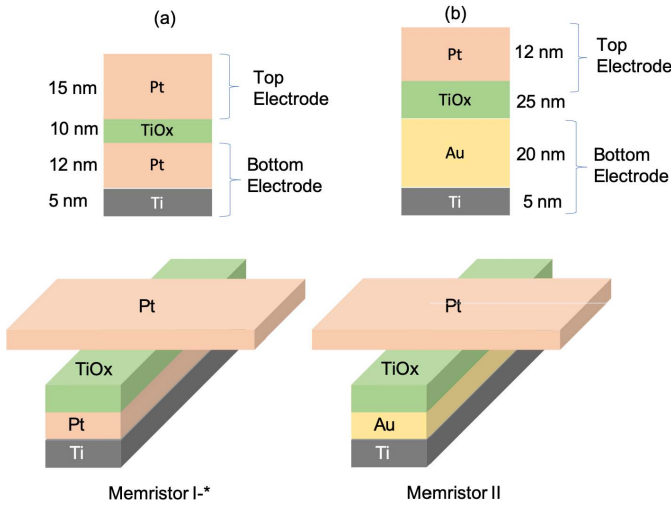


Fig. 1. Schematics of (a) memristor I-* and (b) memristor II with the information of thickness of each layer.

This article is the first of a two-part series: in part I, we demonstrate a methodology for extracting behavioral models for the switching dynamics of TiO_x memristors including temperature dependence. We also show a simple technique used to reduce the model parameter size. In part II, we propose a physics-based model for the temperature dependence, where physical realism has been stressed over performance.

II. EXPERIMENTAL METHODS

In this work, we have used two different types of TiO_x -based memristor devices. Schematic representation of both the type of memristor devices is shown in Fig. 1. memristors I-a and I-b (jointly referred to as memristor I-* in the remainder of this article) are Pt/ TiO_x /Pt with Pt as the top and bottom electrode and memristor II is Pt/ TiO_x /Au with Pt as the top electrode and Au as the bottom electrode. Both types of devices are fabricated on two separate 6-in oxidized (200-nm dry oxide, i.e., SiO_2) silicon wafers. Bottom electrodes are defined using photolithography followed by e-beam evaporation of adhesive 5-nm Ti layer and then 12-nm Pt (20-nm Au) for memristor I-* (memristor II). This deposition is followed by lift-off process in N-methyl-2-pyrrolidone (NMP). Followed by subsequent photolithography, a TiO_x active layer of thickness 10 nm (25 nm) for memristor I-* (memristor II) is then deposited using reactive magnetron sputtering of Ti target. Lift-off process was then carried out using NMP followed by photolithography for the top electrode. The e-beam evaporation of 15-nm Pt (12-nm Pt) for memristor I-* (memristor II) and lift-off processes are then carried out.

For electrical characterization, we use an Arc One from Arc Instruments [18], [19]. The electrical characterization of both types of memristors is conducted on $20 \mu\text{m} \times 20 \mu\text{m}$ devices defined by overlapping cross patterned electrodes as shown in Fig. 1. To achieve memristive operation in our TiO_x devices, we use a pulse-based electroforming protocol [20], [21]. And then, to obtain the PRT characteristics, we apply a train of pulses of fixed amplitude. The amplitude of the pulse train

is swept across biases in the switching regime and at each bias step, both polarities are visited. An example of such a bias sequence is 0.8, -0.8 , 0.9, -0.9 , 1.0, and -1.0 V. In this article, the application of train of pulses at a particular amplitude is referred to as the switching bias. Each switching bias consists of 500 pulses (for memristor I-*) and 200 pulses (for memristor II) of 100- μs pulsewidth. In between the consecutive programming pulses, a read pulse of 200 mV is applied to measure the resistance of the device. Since the model presented in this work is intended for application in nonvolatile memristors, for a short interpulse and read pulse duration, device retention is guaranteed and device resistance is unchanged. Fig. 2 shows the biasing protocol employed in the PRT measurements. Fig. 2(a) shows the typical response of a memristor device observed in PRT measurements. Fig. 2(b) shows the typical sequence of switching biases employed in the PRT measurements and the outset of the figure shows pulse and read scheme which constitute as an elementary unit of the pulse train. For memristor I-b and for memristor II, we have also performed PRT measurements at temperatures ranging from 313–353 and 300–360 K correspondingly. For memristor I-b, these temperature-dependent measurements are achieved using a chuck-based temperature controller, whereas for memristor II, a microchamber-based temperature control system [22] is used.

III. SWITCHING DYNAMICS MODEL

In the switching regime, voltage biases between the top and bottom electrodes greatly exceed the read-out voltage: $|V| > |V_{\text{read}}|$. If sufficiently high, this voltage may cause the resistance of the memristive device to change. In the case of pulse train stimulation, it is typical that the first switching pulse will change the resistive state significantly with consecutive pulses adding increasingly small increments (or decrements) to the resistance value. This saturation effect can be seen in Fig. 2(a) and provides a natural bound on dR/dt and it is described by an exponential decay. The similar PRT behavior is reported in [13] and [14], however instead of applying the exponential on the absolute resistance, we use the change in resistance versus an initial reference point

$$\Delta R = R - R_0 \quad (1)$$

where R_0 is the resistance value of the memristor before the application of switching bias. The rate of change of the “ R_0 -referred resistance difference” is now modeled by

$$\frac{d\Delta R}{dt} = s(V, T) \exp\left(\frac{\Delta R}{R_p(V, T)}\right) + \frac{d\Delta R}{dt}\Big|_{t=0^-} \quad (2)$$

where s and R_p are the fitting parameters. V is the magnitude of switching bias and T is the temperature. If we assume that prior to applying the switching bias, memristor has reached equilibrium or steady state, then $d\Delta R/dt|_{t=0^-} = 0$. Then, the solution to (2) is

$$\Delta R(t) = -R_p \ln\left(\frac{-st}{R_p} + \exp\left(\frac{-\Delta R_0}{R_p}\right)\right) \quad (3)$$

where ΔR_0 is the initial discrepancy from R_0 . For the switching bias which consists of pulse trains, (3) can be expanded

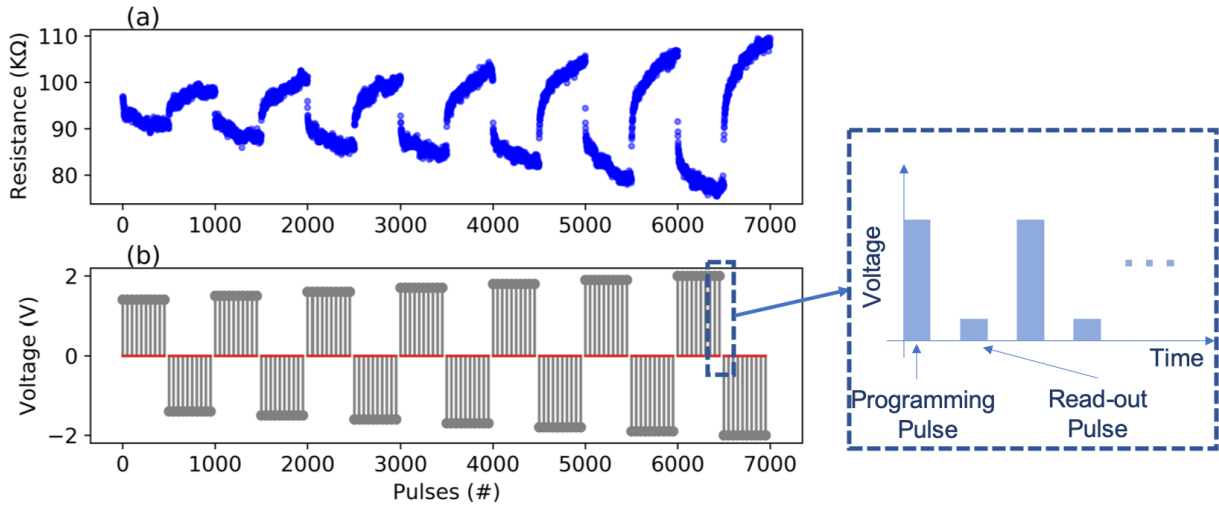


Fig. 2. Basic experimental protocols. (a) Typical response of a memristor device to the “pulse-measure” approach where programming pulses intended to elicit a change in memristor resistive state and read-out pulses intended to assess the resistive state at a standard voltage are kept separate. (b) Corresponding set of pulse trains of increasing amplitudes and alternating polarities used to assess memristor reaction to voltages of different magnitudes.

to express the resistance at the end of the n th pulse as

$$\begin{aligned} \Delta R_n &= -R_p \ln \left(\frac{-st_w}{R_p} + 1 \right), \quad \text{for } n = 1 \\ \Delta R_n &= -R_p \ln \left(\frac{-st_w}{R_p} + \exp \left(\frac{-\Delta R_{n-1}}{R_p} \right) \right), \quad \text{for } n > 1 \end{aligned} \quad (4)$$

where t_w is the pulsewidth. For the very first pulse in the switching bias, initial relative resistance is zero, that is, $\Delta R_0 = 0$. Note that this “ R_0 -referred resistance empirical model” uses two parameters, whereas the previous models used three parameters [13], [14]. This impacts the overall parameter space significantly as we shall see in the next section, which discusses the bias and temperature dependence of the model parameters and how to establish these relationships using a multistage methodology.

IV. MODEL FITTING METHODOLOGY

The parameters s and R_p presented in (2) have a dependence on temperature and applied switching bias. To establish the nature of $s(V, T)$ and $R_p(V, T)$, we use a three-stage methodology as illustrated in Fig. 3. With every stage, the size of the parameter space expands. In this methodology, except for stage I, the mathematical expressions used to expand the parameter space are not assumed *a priori*. Rather, an appropriate mathematical expression is chosen based on the extracted parameters from the previous stage. Initially, pulsed transients of ΔR measured at a range of temperatures are fitted at each switching bias independently. With this, we obtain a scatter of s and R_p for various temperatures and switching biases. In stage II, the functional shape of bias dependence is established for each temperature, that is, we look at how s and R_p vary with bias, establish the functional form of this dependence, and extract parameters for each temperature. In stage III, we determine the temperature dependence of the

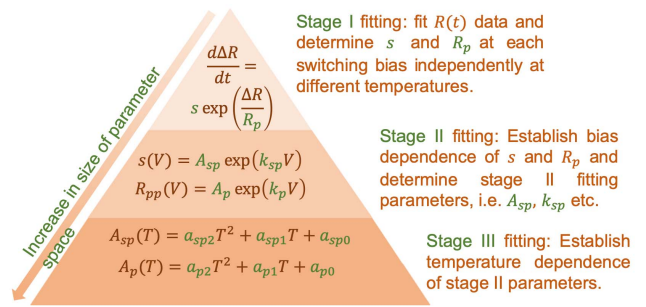


Fig. 3. Multistage fitting methodology employed for the parameter extraction of the temperature-dependent switching dynamics model.

parameters extracted during stage II. This process is repeated for each voltage bias and polarity.

Depending on the mathematical functions used at each stage, the parameter space may expand to a very large one. The number of parameters expands in a multiplicative manner at each stage, and therefore it is important for computational efficiency to reduce the number of parameters at all stages of the methodology. Previous work uses a three-parameter model in (2), ending up with a parameter space of $3 \times 2 \times 3 = 18$ parameters/polarity (ppp). As we discuss in the next section, we use a two-parameter model in (3), reducing the total size of the parameter space to $2 \times 2 \times 3 = 12$ ppp and increasing computational efficiency.

V. RESULTS AND DISCUSSION

In this section, we present our switching dynamics models for memristor I-* and memristor II. We begin with demonstrating our new switching dynamics model at room temperature on memristor I-a. For this, we measure PRT as in Fig. 2. Switching biases of 1.4–2.0 V of alternate polarity are applied consecutively for 20 times on memristor I-a to check model robustness. The PRT and stage I fitting are shown in Fig. 4. Note that, in Fig. 4(a), the pulsed transients of ΔR are shown

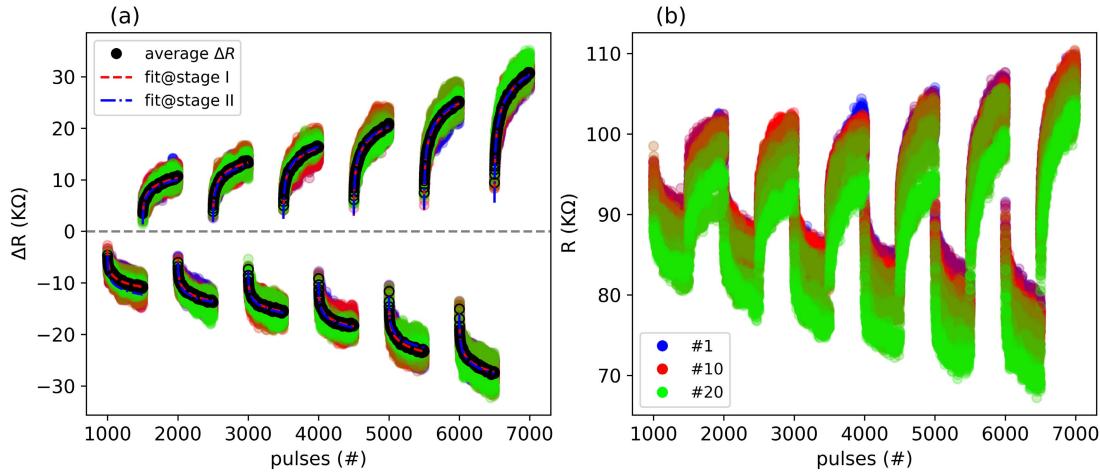


Fig. 4. PRT measurements on memristor I-a. The switching bias amplitude is swept from 1.4 to 2.0 V with a step size of 0.04 V. The switching bias polarity is altered for each amplitude as illustrated in Fig. 2. Each switching bias consists of 500 pulses of 100 μ s and 10-ms interpulse. (a) Pulsed transients of the change in resistance for 20 consecutive measurements and their average (black symbols). Model fits at stages I and II are also shown. (b) Pulsed transients of absolute device resistance.

with the corresponding absolute resistance values shown in Fig. 4(b). Even though the values of absolute resistance do change in consecutive measurements, ΔR does not (to within approximation). Therefore, if we fit the model to the average values of the ΔR transients, we can obtain a robust set of model parameters.

The fittings to the average of pulsed transients of ΔR for memristor I-a at stages I and II are shown in Fig. 4(a). The average of ΔR is obtained from 20 consecutive PRT measurements data shown in Fig. 4(b). Stage I fitting yields the parameter values (s and R_p) at the measured switching biases. Then, in order to establish the bias dependence of s and R_p , we use the exponential expression for s and second-order polynomials for R_p in stage II as follows:

$$s = s_A \exp(s_k V) \quad (5)$$

$$R_p = p_2 V^2 + p_1 V + p_0. \quad (6)$$

Fig. 4(a) shows the fitting of pulsed transients of relative resistance at the switching biases of ± 1.4 to ± 2.0 V swept with a ± 0.04 -V step size. Fig. 5(a)–(d) shows the bias dependence of s and R_p and the corresponding fits using (5) and (6). Fig. 4(a) also shows the simulated pulsed transients of relative resistance using stage II fitting parameters, that is, s_A , s_k , p_0 , p_1 , and p_2 . It can be seen that the simulated pulsed ΔR transients match very well to the average of the pulsed transients of ΔR and the stage I fit. Model parameters for memristor I-a are summarized in Table I.

Fig. 6 presents the comparison of previous work [14] and this work. Fig. 6(a) shows the model fittings at stage I in both the works. We can notice that both the model fittings overlap, indicating that there is negligible difference. The percentage fitting error is presented in Fig. 6(b). Obviously, both the models present no difference in the fitting error. The maximum error at stage I is nearly 5% in both the models. Given that the error difference between the two models is negligible, the two-parameter model presented in this work has an obvious advantage in terms of computational efficiency over the previous three parameter model.

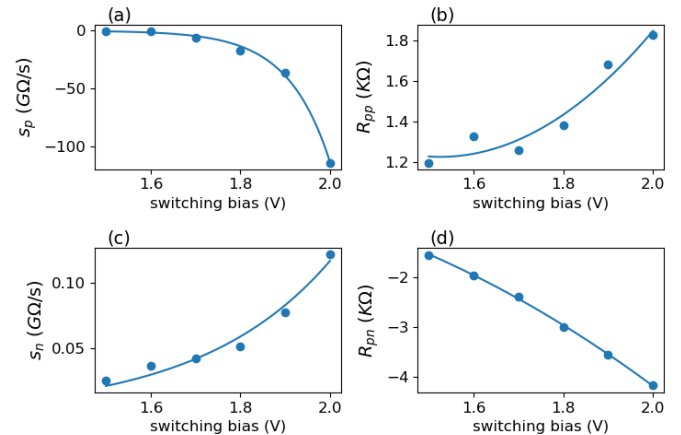


Fig. 5. Stage II fitting process: Bias dependence of fitting parameters extracted from stage I. (a) s and (b) R_p for positive polarity switching biases and (c) s , and (d) R_p for negative polarity switching biases. The subscript “p” (“n”) as in s_p (s_n) and R_{pp} (R_{pn}) is used to indicate positive polarity (negative polarity).

We now illustrate the switching dynamics model for memristor II. Fig. 7 shows the PRT characteristics measured at different temperatures from 300 to 360 K. It can be observed from Fig. 7(a)–(g) that the absolute resistance of the device decreases with the increase in temperature. We observe such a trend in all our TiO_x devices. This thermal behavior is a result of Schottky conduction mechanism and is discussed in detail in the part II of the series. Fig. 7(h) also shows the stage I model fit to the PRT characteristics at the corresponding temperatures. Fig. 8 shows $s(V)$ and $R_p(V)$ plotted at various temperatures. For memristor II, the bias dependence of s (at different temperatures) for both positive and negative switching biases is modeled as constant. The average values are used as the stage II model parameters. $R_p(V)$ are modeled using exponentials as

$$R_p(V, T) = A(T) \exp(k(T)V). \quad (7)$$

The stage III fittings to $s(T)$, $A(T)$, and $k(T)$ are shown in Fig. 9. Second-order polynomials are used to parameterize

TABLE I
MODEL SUMMARY OF MEMRISTOR I-a

Stage	Equations	Parameter	Positive Polarity Value	Negative Polarity Value	Units
stage I	$d\Delta R/dt = s \exp(\Delta R/R_p)$	s_A	-6.054×10^{-2}	123.9	$\text{K}\Omega/\text{s}$
stage II	$s(V) = s_A \exp(s_k V)$ $R_p(V) = p_2^{R_p} V^2 + P_1^{R_p} V + p_0$	s_k	10.67	3.423	V^{-1}
		$p_2^{R_p}$	2.758	-2.723	$\text{K}\Omega/\text{V}^2$
		$P_1^{R_p}$	-8.412	4.229	$\text{K}\Omega/\text{V}$
		$P_0^{R_p}$	7.641	1.749	$\text{K}\Omega$

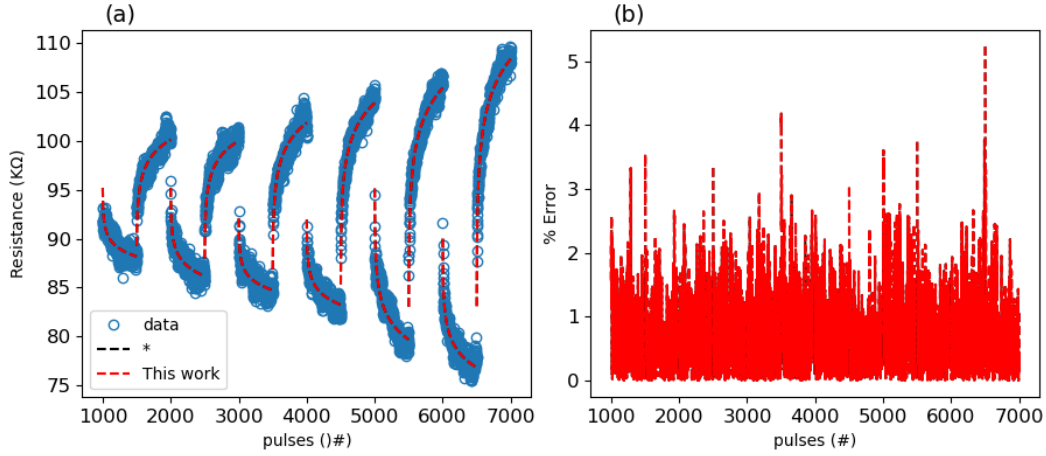


Fig. 6. Comparison of the previous model ([14]) and this work. (a) Stage I fitting of both the models to the PRT data at first instance of the 20 consecutive measurements. (b) Comparison of the model error. In (a) and (b), red dashed line and black dashed line overlap indicating that there is a negligible difference between both the models.

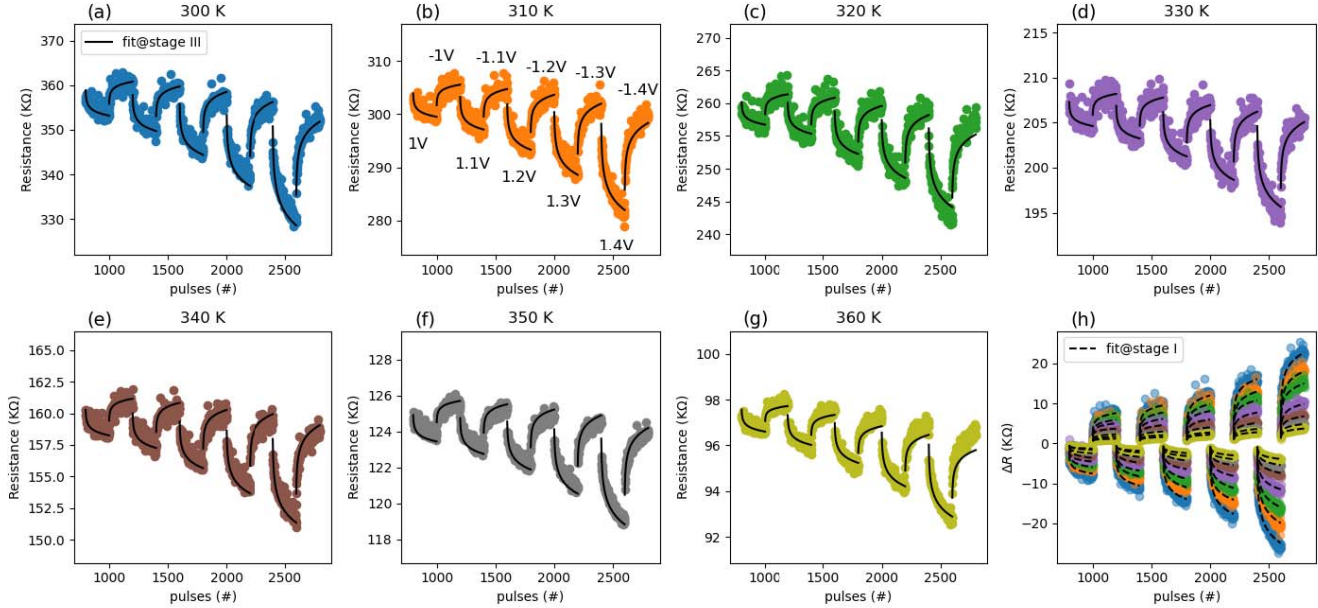


Fig. 7. PRT measurement data of memristor II at temperatures (a) 300 K, (b) 310 K, (c) 320 K, (d) 330 K, (e) 340 K, (f) 350 K, and (g) 360 K. (h) Pulsed transients of relative resistance corresponding to the PRT data shown in (a)–(g). In (h), stage I model fit to the data is also shown with dashed lines. (a)–(g) PRT simulation using extracted stage III model parameters; solid line overlaid on PRT data.

their temperature dependence. Second-order polynomials are used for its generic applicability and simplicity; however, this strictly data-driven approach in using polynomials would impose limitations on extrapolating outside of fitted range. For example, extrapolating $s_{p,n}(T)$ and $A_{p,n}(T)$ to very high

temperatures might change the sign, suggesting that model would no longer be applicable beyond a certain temperature. All the coefficients of these second-order polynomials constitute a full temperature-dependent switching dynamics model of memristor II. Therefore, at this final stage of the

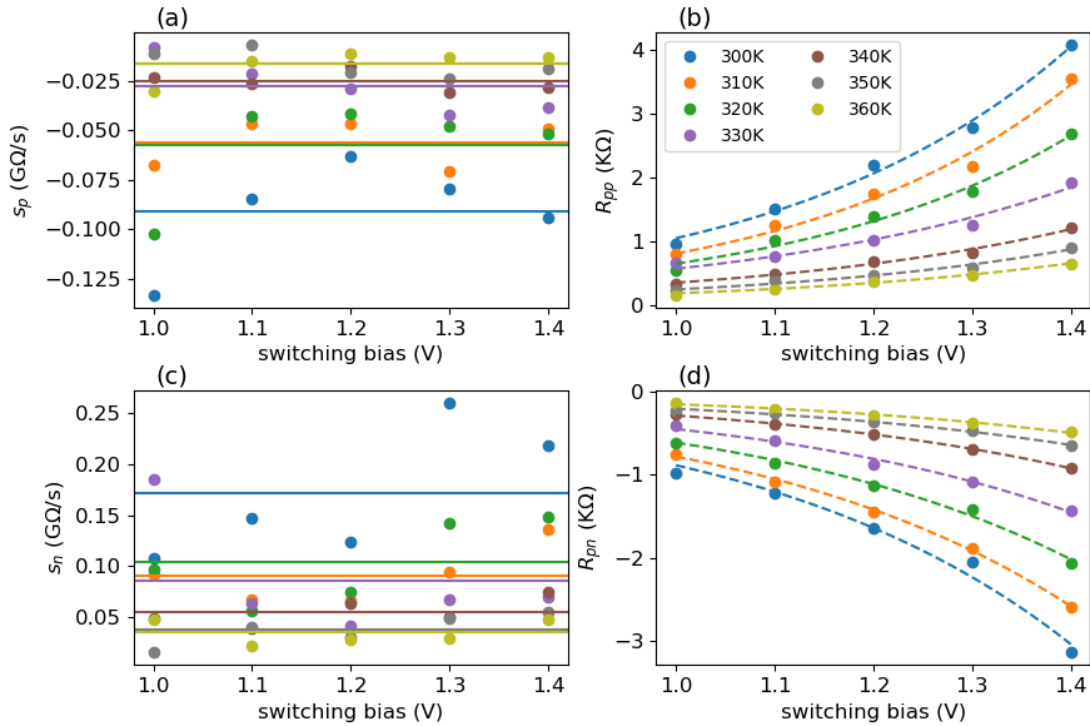


Fig. 8. (a)–(d) Parameterization of stage I parameters (s_p , s_n , R_{pp} , and R_{pn}) to determine the bias dependence. The bias dependence of s_p and s_n is modeled as constant and the average values are used as the stage II model parameters. R_{pp} and R_{pn} are observed to be exponentially dependent on the applied switching bias.

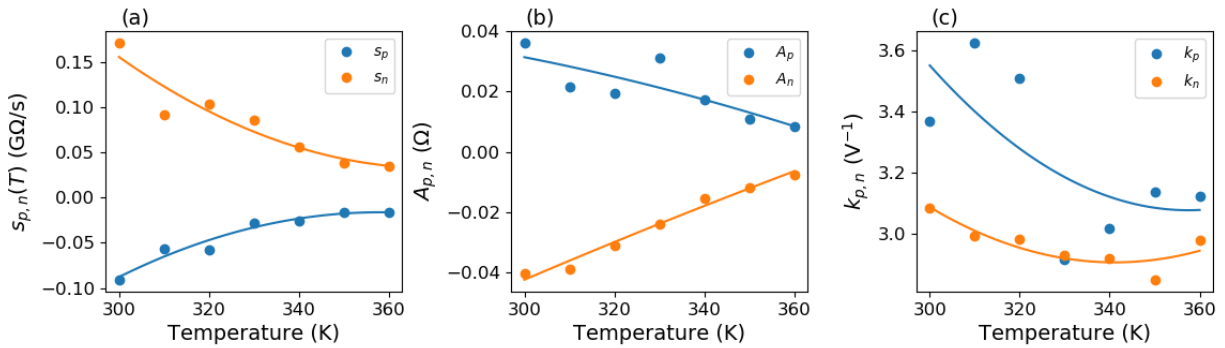


Fig. 9. (a)–(c) Stage III fittings of the stage II model parameters of memristor II. For each stage II parameter, temperature dependence is established using second-order polynomials. The coefficients of these second-order polynomials completely describe the model.

modeling methodology, we must simulate the PRT entirely using the stage III parameters and compare it with the PRT data. The resistance transient characteristics determined by only using the stage III parameters are plotted (with solid black line) in Fig. 7(a)–(g). It can be seen that the simulated characteristics are well matched with the measured experimental data. $s(V, T)$ is not expanded in stage II and modeled as a scalar value equaling the average of all stage I values. In stage III, the thermal dependence of $s(V, T)$ is modeled as a second-order polynomial. Therefore, modeling of $s(V, T)$ takes in total $1 \times 1 \times 3 = 3$ ppp. On the other hand, $R_p(V, T)$ is modeled as a two-parameter exponential mentioned in (6) in stage II and then thermal dependence of each stage II parameter ($A(T)$ and $\kappa(T)$) is modeled with a three-parameter second-order polynomial. Therefore,

the modeling of $R_p(V, T)$ takes $1 \times 2 \times 3 = 6$ ppp. The final size of the parameter space at the end of the stage III for memristor II is 9 ppp. The model summary for memristor II is presented in Table II. These parameters can be used in verilog-A for circuit design.

We also present a fitted compact model for memristor I-b. Model fittings at stages I and III are shown in Fig. 10. We observe that the model describes the PRT behavior of memristor I-b well. At 313 and 353 K, the model predictions for positive polarity switching biases seem to produce significant errors at stage III, whereas stage I fitting errors are within reasonable limits [Fig. 10(f)]. This increase of the fitting error can be due to outliers in the $s(V, T)$ and $R_p(V, T)$ scatter obtained in stage I. Model parameters for memristor I-b are summarized in Table III.

TABLE II
MODEL SUMMARY OF MEMRISTOR II

Stage	Equations	Parameter	Positive Polarity Value	Negative Polarity Value	Units
stage I	$d\Delta R/dt = s \exp(\Delta R/R_p)$	$p_2^{s_0}$	-2.122×10^1	2.493×10^1	$\text{K}\Omega/\text{K}^2\text{s}$
stage II	$s(V, T) = s_0(T)$	$p_1^{s_0}$	1.520×10^4	-1.846×10^4	$\text{K}\Omega/\text{Ks}$
	$R_p(V, T) = A(T) \exp(k(T)V)$	$p_0^{s_0}$	-2.737×10^6	3.450×10^6	$\text{K}\Omega/\text{s}$
stage III	$s_0(T) = p_2^{s_0}T^2 + p_1^{s_0}T + p_0^{s_0}$	p_2^A	-1.478×10^{-6}	-6.147×10^{-7}	$\text{K}\Omega/\text{K}^2$
	$A(T) = p_2^A T^2 + p_1^A T + p_0^A$	p_1^A	5.930×10^{-4}	1.007×10^{-3}	$\text{K}\Omega/\text{K}$
	$k(T) = p_2^k T^2 + p_1^k T + p_0^k$	p_0^A	-1.348×10^{-2}	-2.892×10^{-1}	$\text{K}\Omega$
		p_2^k	1.432×10^{-4}	1.068×10^{-4}	$\text{V}^{-1}\text{K}^{-2}$
		p_1^k	-1.024×10^{-1}	-7.286×10^{-2}	$\text{V}^{-1}\text{K}^{-1}$
		p_0^k	2.138×10^1	1.533×10^1	V^{-1}

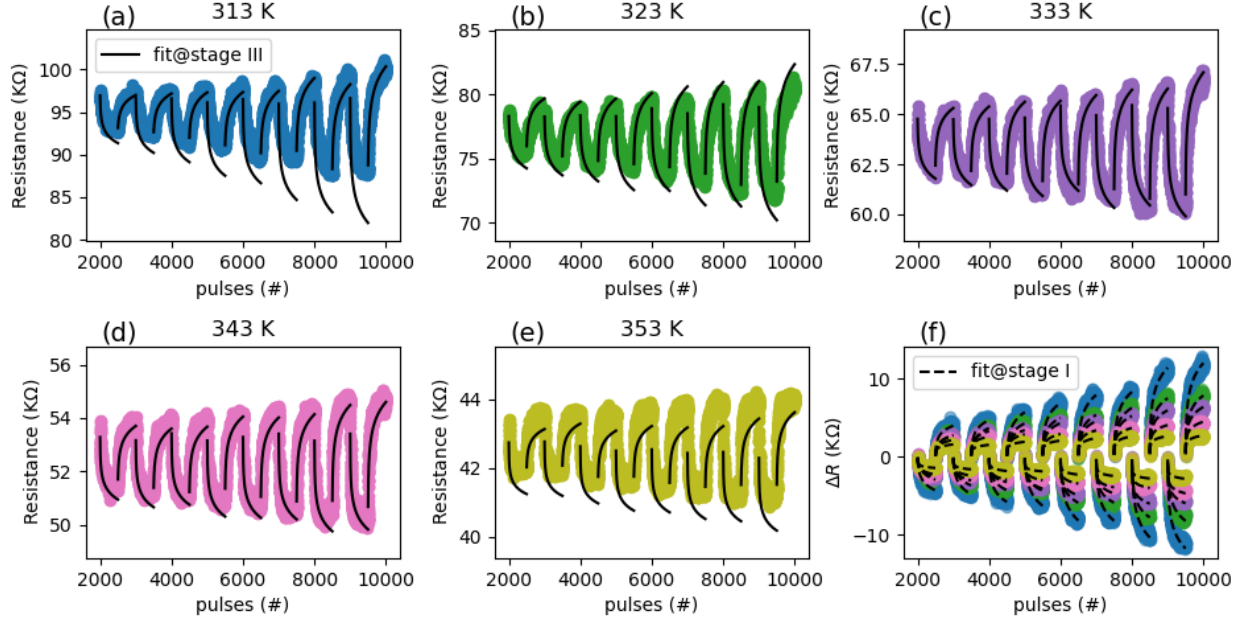


Fig. 10. Model fitting for memristor I-b. PRT characteristics and model fitting at stage III are shown in (a) for 313 K, (b) 323 K, (c) 333 K, (d) 343 K, and (e) 353 K. (f) Pulsed transients of relative resistance and model fittings at stage I. Applied switching bias sequence for PRT measurements is (0.88, -0.88, 0.92, -0.92, 0.96, -0.96, 1, -1, 1.04, -1.04, 1.08, -1.08, 1.12, -1.12, 1.16, -1.16) V.

TABLE III
MODEL SUMMARY OF MEMRISTOR I-b

Stage	Equations	Parameter	Positive polarity value	Negative polarity value	Units
stage I	$d\Delta R/dt = s \exp(\Delta R/R_p)$	$p_1^{s_A}$	-1.384×10^{-1}	9.254×10^{-2}	$\text{K}\Omega/\text{Ks}$
stage II	$s(V, T) = s_A(T) \exp(s_k V)$	$p_0^{s_A}$	4.125×10^1	-2.618×10^1	$\text{K}\Omega/\text{s}$
	$R_p(V, T) = R_{pA}(T) \exp(R_{pk}(T)V)$	$p_2^{s_k}$	5.332×10^{-3}	-1.596×10^{-3}	$\text{V}^{-1}\text{K}^{-2}$
stage III	$s_A(T) = p_1^{s_A} T + p_0^{s_A}$	$p_1^{s_k}$	-3.534×10^0	1.018×10^0	$\text{V}^{-1}\text{K}^{-1}$
	$s_k(T) = p_2^{s_k} T^2 + p_1^{s_k} T + p_0^{s_k}$	$p_0^{s_k}$	5.928×10^2	-1.559×10^2	V^{-1}
	$R_{pA}(T) = p_2^{R_{pA}} T^2 + p_1^{R_{pA}} T + p_0^{R_{pA}}$	$p_2^{R_{pA}}$	-1.770×10^{-4}	1.378×10^{-4}	$\text{K}\Omega/\text{K}^2$
	$R_{pk}(T) = p_2^{R_{pk}} T^2 + p_1^{R_{pk}} T + p_0^{R_{pk}}$	$p_1^{R_{pA}}$	1.178×10^{-1}	-9.155×10^{-2}	$\text{K}\Omega/\text{K}$
		$p_0^{R_{pA}}$	-1.943×10^1	1.510×10^1	$\text{K}\Omega$
		$p_2^{R_{pk}}$	1.229×10^{-3}	1.204×10^{-3}	$\text{V}^{-1}\text{K}^{-2}$
		$p_1^{R_{pk}}$	-8.606×10^{-1}	-8.383×10^{-1}	$\text{V}^{-1}\text{K}^{-1}$
		$p_0^{R_{pk}}$	1.518×10^2	1.476×10^2	V^{-1}

VI. CONCLUSION

We have presented a methodology for extracting improved switching dynamics models for memristive devices and demonstrate how it is used to extract models for two memristive devices. The methodology can be used to extract thermal characteristics of resistive switching, which previous works did not include. We observe that although the absolute values

of the resistance change in the consecutive measurements, the “ R_0 -referred” change in resistance does not, thus giving rise to a robust switching dynamics model. This technique also reduces the size of the parameter space at a fundamental level, that is, in stage I of the fitting methodology, making the model intrinsically more computationally efficient. The switching dynamics is modeled purely behaviorally in this work, using

a multistage fitting methodology to extract the complete set of model parameters. Since the bias and temperature dependence of the model parameters is not assumed *a priori* and instead allowed to emerge through a multistage methodology, the behavioral modeling methodology is generally applicable and can in principle be used for different types of TiO_x memristors.

REFERENCES

- [1] D. B. Strukov, G. S. Snider, D. R. Stewart, and R. S. Williams, "The missing memristor found," *Nature*, vol. 453, no. 7191, p. 80, May 2008, doi: [10.1038/nature06932](https://doi.org/10.1038/nature06932).
- [2] M.-J. Lee *et al.*, "A fast, high-endurance and scalable non-volatile memory device made from asymmetric $\text{Ta}_2\text{O}_{5-x}/\text{TaO}_{2-x}$ bilayer structures," *Nature Mater.*, vol. 10, no. 8, pp. 625–630, Aug. 2011. [Online]. Available: <https://www.nature.com/articles/nmat3070>
- [3] S. B. Eryilmaz, D. Kuzum, S. Yu, and H.-S.-P. Wong, "Device and system level design considerations for analog-non-volatile-memory based neuromorphic architectures," in *IEDM Tech. Dig.*, Dec. 2015, pp. 4.1.1–4.1.4, doi: [10.1109/IEDM.2015.7409622](https://doi.org/10.1109/IEDM.2015.7409622).
- [4] A. Serb, J. Bill, A. Khiat, R. Berdan, R. Legenstein, and T. Prodromakis, "Unsupervised learning in probabilistic neural networks with multi-state metal-oxide memristive synapses," *Nature Commun.*, vol. 7, no. 1, p. 12611, Sep. 2016, doi: [10.1038/ncomms12611](https://doi.org/10.1038/ncomms12611).
- [5] I. Gupta, A. Serb, A. Khiat, R. Zeitler, S. Vassanelli, and T. Prodromakis, "Real-time encoding and compression of neuronal spikes by metal-oxide memristors," *Nature Commun.*, vol. 7, no. 1, p. 12805, Sep. 2016, doi: [10.1038/ncomms12805](https://doi.org/10.1038/ncomms12805).
- [6] S. Yu, Y. Wu, R. Jeyasingh, D. Kuzum, and H.-S. P. Wong, "An electronic synapse device based on metal oxide resistive switching memory for neuromorphic computation," *IEEE Trans. Electron Devices*, vol. 58, no. 8, pp. 2729–2737, Aug. 2011, doi: [10.1109/TED.2011.2147791](https://doi.org/10.1109/TED.2011.2147791).
- [7] S. Yu, B. Gao, Z. Fang, H. Yu, J. Kang, and H.-S. P. Wong, "A low energy oxide-based electronic synaptic device for neuromorphic visual systems with tolerance to device variation," *Adv. Mater.*, vol. 25, no. 12, pp. 1774–1779, Jan. 2013, doi: [10.1002/adma.201203680](https://doi.org/10.1002/adma.201203680).
- [8] J. Liu *et al.*, "An electronic synaptic device based on $\text{HfO}_2/\text{TiO}_x$ bilayer structure memristor with self-compliance and deep-RESET characteristics," *Nanotechnology*, vol. 29, no. 41, Aug. 2018, Art. no. 415205, doi: [10.1088/1361-6528/aad64d](https://doi.org/10.1088/1361-6528/aad64d).
- [9] G. Papandroulidakis, I. Vourkas, N. Vasileiadis, and G. C. Sirakoulis, "Boolean logic operations and computing circuits based on memristors," *IEEE Trans. Circuits Syst. II, Exp. Briefs*, vol. 61, no. 12, pp. 972–976, Dec. 2014, doi: [10.1109/TCSII.2014.2357351](https://doi.org/10.1109/TCSII.2014.2357351).
- [10] G. Papandroulidakis, A. Serb, A. Khiat, G. V. Merrett, and T. Prodromakis, "Practical implementation of memristor-based threshold logic gates," *IEEE Trans. Circuits Syst. I, Reg. Papers*, vol. 66, no. 8, pp. 3041–3051, Aug. 2019, doi: [10.1109/TCSI.2019.2902475](https://doi.org/10.1109/TCSI.2019.2902475).
- [11] S.-Y. Hu *et al.*, "Reconfigurable Boolean logic in memristive crossbar: The principle and implementation," *IEEE Electron Device Lett.*, vol. 40, no. 2, pp. 200–203, Feb. 2019, doi: [10.1109/LED.2018.2886364](https://doi.org/10.1109/LED.2018.2886364).
- [12] Y. N. Joglekar and S. J. Wolf, "The elusive memristor: Properties of basic electrical circuits," *Eur. J. Phys.*, vol. 30, no. 4, pp. 661–675, May 2009. [Online]. Available: <https://iopscience.iop.org/article/10.1088/0143-0807/30/4/001>
- [13] C. Yakopcic, T. M. Taha, G. Subramanyam, and R. E. Pino, "Generalized memristive device SPICE model and its application in circuit design," *IEEE Trans. Comput.-Aided Design Integr. Circuits Syst.*, vol. 32, no. 8, pp. 1201–1214, Aug. 2013, doi: [10.1109/TCAD.2013.2252057](https://doi.org/10.1109/TCAD.2013.2252057).
- [14] I. Messaris, A. Serb, S. Stathopoulos, A. Khiat, S. Nikolaidis, and T. Prodromakis, "A data-driven Verilog-A ReRAM model," *IEEE Trans. Comput.-Aided Design Integr. Circuits Syst.*, vol. 37, no. 12, pp. 3151–3162, Dec. 2018, doi: [10.1109/TCAD.2018.2791468](https://doi.org/10.1109/TCAD.2018.2791468).
- [15] S. Kvatinisky, M. Ramadan, E. G. Friedman, and A. Kolodny, "VTEAM: A general model for voltage-controlled memristors," *IEEE Trans. Circuits Syst. II, Exp. Briefs*, vol. 62, no. 8, pp. 786–790, Aug. 2015, doi: [10.1109/TCSII.2015.2433536](https://doi.org/10.1109/TCSII.2015.2433536).
- [16] T. Chang, S.-H. Jo, K.-H. Kim, P. Sheridan, S. Gaba, and W. Lu, "Synaptic behaviors and modeling of a metal oxide memristive device," *Appl. Phys. A, Solids Surf.*, vol. 102, no. 4, pp. 857–863, Mar. 2011, doi: [10.1007/s00339-011-6296-1](https://doi.org/10.1007/s00339-011-6296-1).
- [17] M. D. Pickett *et al.*, "Switching dynamics in titanium dioxide memristive devices," *J. Appl. Phys.*, vol. 106, no. 7, Oct. 2009, Art. no. 074508, doi: [10.1063/1.3236506](https://doi.org/10.1063/1.3236506).
- [18] ArcOne Measurement Board. Accessed: Jun. 29, 2020. [Online]. Available: <https://www.arc-instruments.co.uk/products/arc-one/>
- [19] R. Berdan, A. Serb, A. Khiat, A. Regoutz, C. Papavassiliou, and T. Prodromakis, "A μ -controller-based system for interfacing selectorless RRAM crossbar arrays," *IEEE Trans. Electron Devices*, vol. 62, no. 7, pp. 2190–2196, Jul. 2015, doi: [10.1109/TED.2015.2433676](https://doi.org/10.1109/TED.2015.2433676).
- [20] L. Michalas, S. Stathopoulos, A. Khiat, and T. Prodromakis, "Conduction mechanisms at distinct resistive levels of $\text{Pt}/\text{TiO}_{2-x}/\text{Pt}$ memristors," *Appl. Phys. Lett.*, vol. 113, no. 14, Oct. 2018, Art. no. 143503, doi: [10.1063/1.5040936](https://doi.org/10.1063/1.5040936).
- [21] S. Stathopoulos, L. Michalas, A. Khiat, A. Serb, and T. Prodromakis, "An electrical characterisation methodology for benchmarking memristive device technologies," *Sci. Rep.*, vol. 9, no. 1, p. 19412, Dec. 2019, doi: [10.1038/s41598-019-55322-4](https://doi.org/10.1038/s41598-019-55322-4).
- [22] T. Abbey *et al.*, "An embedded environmental control micro-chamber system for RRAM memristor characterisation," in *Proc. IEEE Int. Symp. Circuits Syst. (ISCAS)*, May 2018, pp. 1–4, doi: [10.1109/ISCAS.2018.8351673](https://doi.org/10.1109/ISCAS.2018.8351673).